CFD Letters www.cfdl.issres.net Vol. 6 (2) – June 2013

A BGK-based Two-Equation Turbulence Model Algorithm for Solving Compressible Navier-Stokes Equations

Jiunn Chit Ong[1], Ashraf A. Omar[2c] and Waqar Asrar[3]
[1] *Faculty of Mechanical Engineering, Universiti Teknologi MARA (Pulau Pinang), MALAYSIA*
[2] *Department of Aeronautical Engineering, Faculty of Engineering, University of Tripoli, LIBYA*
[3] *Department of Mechanical Engineering, Faculty of Engineering, International Islamic University Malaysia, MALAYSIA*

Received: 12/09/2013 – Revised 18/12/2013 – Accepted 19/12/2013

Abstract

The implementation and validation of the *k-ε* / *k-ω* SST (Shear-Stress-Transport) two-equation turbulence model into the existing BGK (Bhatnagaar-Gross-Krook) flow solver for compressible Navier-Stokes equations in two-space dimensions generalized coordinates are presented. In developing the desired algorithm, the convection flux terms are discretized by a semi-discrete finite difference method. Then, the resulting inviscid flux functions are approximated by the gas-kinetic BGK scheme based on the approximate collisional Boltzmann equation. For high-order spatial accuracy, the cell interface values required by the inviscid flux functions are reconstructed via the MUSCL (Monotone Upstream-Centered Schemes for Conservation Laws) variable interpolation method coupled with a minmod limiter. As for the diffusion flux terms, they are discretized with a second-order central difference scheme. An explicit-type time integration method known as the modified fourth-order Runge-Kutta method is used to march the solution to steady-state. Four test cases have been solved using the developed algorithm, namely turbulent flat plate, transitional flat plate, turbulent RAE2822 airfoil and turbulent Sajben diffuser flows. The accuracy of the solver is examined and results obtained from the computations are also compared with available experimental or analytical data that will demonstrate good agreement has been obtained.

Keywords: Finite difference; gas-kinetic BGK scheme; Navier-Stokes equations; turbulence model; Boltzmann Model; MUSCL; modified fourth-order Runge-Kutta.

1. Introduction

In the development of flow solvers for practical gas dynamics applications, the key design criterion is to maximize robustness and accuracy. This requirement is particularly important in

[c] Corresponding Author: Ashraf A. Omar
Email: aao@iium.edu.my Telephone: +603 61964486
 PI: S2180-1363(14)6046-X

compressible flows involving high-speed flow where intense shock waves and boundary layers may simultaneously exist. Among those notable and successful are the Godunov-type and flux vector splitting schemes. Besides these schemes, gas-kinetic schemes have attracted much attention in recent years due to their superior accuracy, robustness and good resolution characteristics over conventional schemes.

Recent developments have seen the emergence of another class of scheme known as the gas-kinetic schemes that are developed based on the Boltzmann equation [1, 2]. Mainly, there are two groups of gas-kinetic schemes and the difference lies within the type of Boltzmann equation use in the gas evolution stage. One of them is the well-known KFVS (Kinetic Flux Vector Splitting) scheme which is based on the collisionless Boltzmann equation and the other is based on the collisional BGK model [3] where the BGK scheme is derived. Like any other FVS (Flux Vector Splitting) method, the KFVS scheme is very diffusive and less accurate in comparison with the Roe-type FDS (Flux Difference Splitting) method. The diffusivity of the FVS schemes is mainly due to the particle or wave-free transport mechanism, which sets the CFL (Courant–Friedrichs–Lewy) time step equal to particle collision time [4]. In order to reduce diffusivity, particle collisions have to be modeled and implemented into the gas evolution stage. One of the distinct approaches to take particle collision into consideration in gas evolution can be found in Ref. [1]. In this method, the collision effect is considered by the BGK model as an approximation of the collision integral in the Boltzmann equation. It is found that this gas-kinetic BGK scheme possesses accuracy that is superior to the flux vector splitting schemes and avoids the anomalies of FDS-type schemes [5-9].

Most of the developments of the gas-kinetic schemes are focused on solving fluid governing equations via the finite volume method. May et al. [10] have applied the gas-kinetic BGK finite volume method for computing three-dimensional transonic flow with unstructured mesh. Zhang et al. [11] have developed a second-order KFVS scheme for shallow water flows in one-dimension space using finite volume method. Xu et al. [12] used BGK scheme cast in a finite volume manner to study complicated flow phenomena that occur in a laminar hypersonic viscous flows, i.e. shock boundary layer interaction, flow separation and viscous/inviscid interaction. These are just a few of the many applications of the gas-kinetic schemes in the finite volume framework. On the other hand, only a limited number of efforts are channeled into the development of the gas-kinetic schemes via the finite difference method. To name a few, Ravichandran [13] in 1997 has developed higher order KFVS algorithms using compact upwind difference operators to compute two-dimensional compressible Euler equations. Omar et al. [14] in 2009 have successfully extended the BGK scheme to solve compressible viscous laminar flow.

Turbulent flow motions occur in vast majority of fluid applications. To name a few: fluid flow in a pipe, flow processes in combustion chamber and even flow over an airfoil will exhibit a chaotic complex motion defined as turbulent flow. The most elegant solution to any turbulent flow is via the Direct Numerical Simulation (DNS) of turbulence. This approach is implemented by discretizing the Navier-Stokes equations with higher-order accurate numerical scheme and solved using extremely fine grid mesh. An alternative approach to the DNS technique would be the adoption of Large Eddy Simulation (LES), which draws the advantages of the direct simulation of turbulence flows and the solution of the Reynolds averaged equations through closure assumptions. Although the popularity of DNS and LES have become noticeable [15-17] due to rapid development of high performance computing technology, the general trend of computing turbulent flows still remain with the solution of Reynolds-Averaged Navier-Stokes (RANS) equations with the inclusion of Reynolds stresses into the original full Navier-Stokes equations. Resolving the turbulent flows via this means proved to be computationally cheaper [18, 19] compare to DNS and LES. The closure equations that provide the additional Reynolds stresses in the RANS equations are calculated from turbulence models.

In the present work, a gas-kinetic BGK-based flow solver is extended from the previous work carried out in Ref. [14] to facilitate the computation of turbulent flow using the RANS equations. In the developed solver, the BGK scheme is used to approximate the convective flux terms, while a

second-order central scheme is used to discretize the diffusive flux terms of the RANS equations, coupled with a combined *k-ε* / *k-ω* SST two-equation turbulence model to provide the required Reynolds stresses to resolve the turbulent flow. The solver is tested with four typical turbulent flow problems ranging from simple to complex flow domain. Hence, the computed results for turbulent flat plate, transitional flat plate, turbulent RAE2822 airfoil and turbulent Sajben diffuser are presented. As for validation purposes, available experimental or analytical data for respective test cases would be used as comparison to the numerical solutions obtained from the solver. The predictions showed that good agreement can be achieved via the flow solver in computing turbulent flow.

2. Governing equations

The two-dimensional normalized compressible RANS equations can be written in the strong conservative form as

$$\frac{\partial W}{\partial t}+\frac{\partial F}{\partial x}+\frac{\partial G}{\partial y}=\frac{\partial F_v}{\partial x}+\frac{\partial G_v}{\partial y} \tag{1}$$

Where

$$W=\begin{bmatrix}\rho\\ \rho U\\ \rho V\\ \rho e\end{bmatrix},\quad F=\begin{bmatrix}\rho U\\ \rho U^2+p\\ \rho UV\\ (\rho e+p)U\end{bmatrix},\quad G=\begin{bmatrix}\rho V\\ \rho UV\\ \rho V^2+p\\ (\rho e+p)V\end{bmatrix},$$

$$F_v=\begin{bmatrix}0\\ \tau_{xx}\\ \tau_{xy}\\ U\tau_{xx}+V\tau_{xy}-q_x\end{bmatrix},\quad G_v=\begin{bmatrix}0\\ \tau_{xy}\\ \tau_{yy}\\ U\tau_{xy}+V\tau_{yy}-q_y\end{bmatrix},$$

$$\tau_{xx}=\frac{\mu}{\mathrm{Re}_\infty}\left(\frac{4}{3}\frac{\partial U}{\partial x}-\frac{2}{3}\frac{\partial V}{\partial y}\right),\quad \tau_{yy}=\frac{\mu}{\mathrm{Re}_\infty}\left(\frac{4}{3}\frac{\partial V}{\partial y}-\frac{2}{3}\frac{\partial U}{\partial x}\right),\quad \tau_{xy}=\frac{\mu}{\mathrm{Re}_\infty}\left(\frac{\partial U}{\partial y}+\frac{\partial V}{\partial x}\right),$$

$$q_x=-\frac{\mu}{\mathrm{Re}_\infty \mathrm{Pr}(\gamma-1)M_\infty^2}\frac{\partial T}{\partial x},\quad q_y=-\frac{\mu}{\mathrm{Re}_\infty \mathrm{Pr}(\gamma-1)M_\infty^2}\frac{\partial T}{\partial y}.$$

With ρ, U, V, p, e and T are the macroscopic density, x-component of velocity, y-component of velocity, pressure, total energy and temperature, respectively. While, τ_{xx}, τ_{xy}, τ_{yy} are the shear stress terms and q_x, q_y are the heat conduction terms. The normalization has been carried out by using the following free stream reference quantities: density ρ_∞, velocity U_∞, pressure $\rho_\infty U_\infty^2$, temperature T_∞, reference length L_∞, reference time L_∞/U_∞ and viscosity μ_∞.

From the perspective of RANS computation, the viscosity μ in the stress terms and the term (μ / Pr) in the heat conduction terms of Eq. (1) are modeled as

$$\begin{aligned}\mu &= \mu_l+\mu_t\\ \frac{\mu}{Pr} &= \left(\frac{\mu}{Pr}\right)_l+\left(\frac{\mu}{Pr}\right)_t\end{aligned} \tag{2}$$

where the subscripts l and t represent laminar and turbulent contributions, respectively. The parameter $(Pr)_t$ is called the turbulent Prandtl number and for air it is generally taken to be 0.9 for wall bounded flows. The closure model chosen to yield the turbulent viscosity μ_t that appears in the RANS equations is the combined k-ε / k-ω SST two-equation turbulence model which is given as

$$\frac{\partial}{\partial t}(\rho k)+\frac{\partial}{\partial x_j}(\rho U_j k)=\frac{\partial}{\partial x_j}\left[(\mu+\sigma_k\mu_t)\frac{\partial k}{\partial x_j}\right]+P_k-\beta^*\rho\omega k \tag{3}$$

$$\frac{\partial}{\partial t}(\rho\omega)+\frac{\partial}{\partial x_j}(\rho U_j\omega)=\frac{\partial}{\partial x_j}\left[(\mu+\sigma_\omega\mu_t)\frac{\partial\omega}{\partial x_j}\right]+2(1-F_1)\rho\sigma_{\omega 2}\frac{1}{\omega}\frac{\partial k}{\partial x_j}\frac{\partial\omega}{\partial x_j}+\frac{\gamma}{\nu}P_k-\beta\rho\omega^2 \tag{4}$$

where the production of turbulence P_k is defined as

$$P_k = \tau_{xx,t}\frac{\partial U}{\partial x} + \tau_{xy,t}\left(\frac{\partial U}{\partial y} + \frac{\partial V}{\partial x}\right) + \tau_{yy,t}\frac{\partial V}{\partial y} \tag{5}$$

$$\tau_{xx,t} = \left(\frac{\mu_t}{\mathrm{Re}_\infty}\right)\left(\frac{4}{3}\frac{\partial U}{\partial x} - \frac{2}{3}\frac{\partial V}{\partial y}\right) - \frac{2}{3}\rho k; \quad \tau_{xy,t} = \left(\frac{\mu_t}{\mathrm{Re}_\infty}\right)\left(\frac{\partial U}{\partial y} + \frac{\partial V}{\partial x}\right); \quad \tau_{yy,t} = \left(\frac{\mu_t}{\mathrm{Re}_\infty}\right)\left(\frac{4}{3}\frac{\partial V}{\partial y} - \frac{2}{3}\frac{\partial U}{\partial x}\right) - \frac{2}{3}\rho k \tag{6}$$

In order to employ the above governing equations for finite difference application in non-regular domain, a transformation from the Cartesian coordinates (x, y) to generalized coordinates (ξ, η) is necessary. The resulting transformation yields the following form for Eq. (1)

$$\frac{\partial \bar{W}}{\partial t} + \frac{\partial \bar{F}}{\partial \xi} + \frac{\partial \bar{G}}{\partial \eta} = \frac{\partial \bar{F}_v}{\partial \xi} + \frac{\partial \bar{G}_v}{\partial \eta} \tag{7}$$

Where

$$\bar{W} = W/J, \quad \bar{F} = \left(\xi_x F + \xi_y G\right)/J, \quad \bar{G} = \left(\eta_x F + \eta_y G\right)/J,$$
$$\bar{F}_v = \left(\xi_x F_v + \xi_y G_v\right)/J, \quad \bar{G}_v = \left(\eta_x F_v + \eta_y G_v\right)/J$$

The metric terms which appear in the above equations are related to the derivatives of x and y by

$$\xi_x = Jy_\eta, \quad \xi_y = -Jx_\eta, \quad \eta_x = -Jy_\xi, \quad \eta_y = Jx_\xi \tag{8}$$

and the Jacobian of transformation is given by

$$J = 1/\left(x_\xi y_\eta - y_\xi x_\eta\right) \tag{9}$$

The manners in which these terms are evaluated are clearly described by Hoffmann and Chiang [20].

Similarly, the closure model in Eq. (3) and (4) cast in generalized coordinates can be expressed as

$$\frac{\partial k}{\partial t} = -U_c\frac{\partial k}{\partial \xi} - V_c\frac{\partial k}{\partial \eta} + \frac{1}{\rho\,\mathrm{Re}_\infty}\left\{\xi_x\frac{\partial}{\partial \xi}\left[\left(\mu + \sigma_k\mu_t\right)\left(\xi_x\frac{\partial k}{\partial \xi} + \eta_x\frac{\partial k}{\partial \eta}\right)\right] + \eta_x\frac{\partial}{\partial \eta}\left[\left(\mu + \sigma_k\mu_t\right)\left(\xi_x\frac{\partial k}{\partial \xi} + \eta_x\frac{\partial k}{\partial \eta}\right)\right]\right.$$
$$\left.\xi_y\frac{\partial}{\partial \xi}\left[\left(\mu + \sigma_k\mu_t\right)\left(\xi_y\frac{\partial k}{\partial \xi} + \eta_y\frac{\partial k}{\partial \eta}\right)\right] + \eta_y\frac{\partial}{\partial \eta}\left[\left(\mu + \sigma_k\mu_t\right)\left(\xi_y\frac{\partial k}{\partial \xi} + \eta_y\frac{\partial k}{\partial \eta}\right)\right]\right\} + \frac{P_k}{\rho} - \beta^*\omega k \tag{10}$$

$$\frac{\partial \omega}{\partial t} = -U_c\frac{\partial \omega}{\partial \xi} - V_c\frac{\partial \omega}{\partial \eta} + \frac{1}{\rho\,\mathrm{Re}_\infty}\left\{\xi_x\frac{\partial}{\partial \xi}\left[\left(\mu + \sigma_\omega\mu_t\right)\left(\xi_x\frac{\partial \omega}{\partial \xi} + \eta_x\frac{\partial \omega}{\partial \eta}\right)\right] + \eta_x\frac{\partial}{\partial \eta}\left[\left(\mu + \sigma_\omega\mu_t\right)\left(\xi_x\frac{\partial \omega}{\partial \xi} + \eta_x\frac{\partial \omega}{\partial \eta}\right)\right]\right.$$
$$\left.\xi_y\frac{\partial}{\partial \xi}\left[\left(\mu + \sigma_\omega\mu_t\right)\left(\xi_y\frac{\partial \omega}{\partial \xi} + \eta_y\frac{\partial \omega}{\partial \eta}\right)\right] + \eta_y\frac{\partial}{\partial \eta}\left[\left(\mu + \sigma_\omega\mu_t\right)\left(\xi_y\frac{\partial \omega}{\partial \xi} + \eta_y\frac{\partial \omega}{\partial \eta}\right)\right]\right\} + \frac{\gamma\rho P_k}{\mu k} - \beta\rho\omega^2$$
$$+\left[2\left(1-F_1\right)\sigma_{\omega 2}\frac{1}{\omega}\right]\left[\left(\xi_x\frac{\partial k}{\partial \xi} + \eta_x\frac{\partial k}{\partial \eta}\right)\left(\xi_x\frac{\partial \omega}{\partial \xi} + \eta_x\frac{\partial \omega}{\partial \eta}\right) + \left(\xi_y\frac{\partial k}{\partial \xi} + \eta_y\frac{\partial k}{\partial \eta}\right)\left(\xi_y\frac{\partial \omega}{\partial \xi} + \eta_y\frac{\partial \omega}{\partial \eta}\right)\right] \tag{11}$$

The closure constants (i.e. σ_k, σ_ω, β, β^* and α) found in Eq. (10) and (11) are provided in Ref. [21]. By using similar transformation procedure as outlined beforehand, the transformed production term P_k of Eq. (5) can be easily derived. Once the turbulent quantities k and ω have been computed from the closure model provided in Eq. (10) and (11), respectively, the following relations are used to determine the turbulent viscosity needed by the RANS equations

$$\mu_t = \frac{\rho a_1 k}{\max\left(a_1\omega, \Omega F_2\right)} \tag{12}$$

Where $a_1 = 0.31$, Ω is the absolute value of vorticity and F_2 is the blending function expressed in the following form

$$\Omega = \left|\xi_x\frac{\partial V}{\partial \xi} + \eta_x\frac{\partial V}{\partial \eta} - \xi_y\frac{\partial U}{\partial \xi} - \eta_y\frac{\partial U}{\partial \eta}\right|, \quad F_2 = \tanh\left\{\left[\max\left(\frac{2\sqrt{k}}{0.09\omega y}, \frac{500\mu}{\rho\omega y^2}\right)\right]^2\right\} \tag{13}$$

3. Numerical methods

For the computation of the convective terms in the RANS equations, they are approximated with a semi-discrete finite difference scheme and the result of such initiative is shown as follow

$$\frac{\partial \bar{F}}{\partial ¶} + \frac{\partial \bar{G}}{\partial ¦} = \frac{\bar{F}_{i+1/2,j} - \bar{F}_{i-1/2,j}}{\Delta ¶} + \frac{\bar{G}_{i,j+1/2} - \bar{G}_{i,j-1/2}}{\Delta ¦} \tag{14}$$

The resulting inviscid flux functions at the cell interfaces are then approximated by the corresponding numerical scheme, i.e. BGK. Since the present study is an extension of the flow solver developed in the previous studies [8, 14] to incorporate two-equation turbulence model (i.e. *k-ε* / *k-ω* SST) into the solver to facilitate the simulation of turbulent flow. The formulations of the BGK scheme to approximate the flux functions found in Eq. (14) would remain totally the same as in the previous studies. Thus, without any due elaboration on the aspects of the development of the BGK scheme. The convective flux function $\bar{F}$ at a given cell interface, expressed in generalized coordinates is outlined directly and can be written as follows

$$\bar{F}_{i+1/2,j} = (1 - ¨)\bar{F}^{e}_{i+1/2,j} + ¨\,\bar{F}^{f}_{i+1/2,j} \tag{15}$$

Where *φ* is an adaptive parameter which is determined via physical flow quantities, the superscripts *e* and *f* correspond to equilibrium and free stream flux functions, respectively. As for the numerical inviscid flux function at the cell interface in the *η*-direction, it is obtained in a similar manner and presented as

$$\bar{G}_{i,j+1/2} = (1 - ¨)\bar{G}^{e}_{i,j+1/2} + ¨\,\bar{G}^{f}_{i,j+1/2} \tag{16}$$

The necessary treatment and formulations required for the calculation of parameter *φ*, equilibrium and free stream flux functions appearing in both Eq. (15) and (16) are explained in details in the previous works and they can be found in Ref. [1, 4, 7].

To increase the spatial accuracy of the BGK scheme to higher-order, the MUSCL approach [22] is adopted together with the usage of a minmod limiter. Hence, the left and right states of the primitive variables *ρ*, *U*, *V*, *p* at a cell interface could be obtained through the non-linear reconstruction of the respective variables and are given as

$$Q_{left} = Q_{i,j} + \frac{1}{2}\Phi\left(\frac{\Delta Q_{i+1/2,j}}{\Delta Q_{i-1/2,j}}\right)\Delta Q_{i-1/2,j}, \quad Q_{right} = Q_{i+1,j} - \frac{1}{2}\Phi\left(\frac{\Delta Q_{i+3/2,j}}{\Delta Q_{i+1/2,j}}\right)\Delta Q_{i+1/2,j} \tag{17}$$

where Q is any primitive and $\Delta Q_{i+1/2,\,j} = Q_{i+1,\,j} - Q_{i,\,j}$. The minmod limiter Φ used in the reconstruction of flow variables in Eq. (17) is given as

$$\Phi(\Delta Q_{ratio}) = \min \mathrm{mod}(1, \Delta Q_{ratio}) = \max[0, \min(1, \Delta Q_{ratio})] \tag{18}$$

Where, the term ΔQ_{ratio} represents the ratio term inside the parentheses of Eq. (17).

The diffusion flux terms appearing in the RANS equations are discretized with a second-order central difference scheme where the approximation is applied at cell interface instead of at cell point in order to avoid the difficulty of evaluating points in the finite difference equations which are outside of the domain. Hence, the discretized diffusion flux terms would take on the following form

$$\left.\frac{\partial \bar{F}_v}{\partial ¶}\right|_{i,j} = \frac{(\bar{F}_v)_{i+1/2,j} - (\bar{F}_v)_{i-1/2,j}}{\Delta ¶}, \text{ and } \left.\frac{\partial \bar{G}_v}{\partial ¦}\right|_{i,j} = \frac{(\bar{G}_v)_{i,j+1/2} - (\bar{G}_v)_{i,j-1/2}}{\Delta ¦} \tag{19}$$

All the terms inside the viscous flux vectors can be defined as a product in the following general form [20]

$$(N)(M_{\cdot}) \tag{20}$$

where, the subscript *ζ* can either be *ξ* or *η* depending on the term considered for the viscous flux vector. Assuming that the first term for the second component of the viscous flux vector $\bar{F}_v$ is represented by the following expression

$$\frac{«}{\mathrm{Re}_\infty J}\left(\frac{4}{3}¶_x^2 + ¶_y^2\right)U_¶ \tag{21}$$

Hence, the terms in Eq. (20) can be written as

$$N = \frac{«}{\mathrm{Re}_\infty J}\left(\frac{4}{3}¶_x^2 + ¶_y^2\right), \; M = U, \text{ and } {}_{\cdot} = ¶ \tag{22}$$

Subsequently, the second-order central difference approximation for the considered term can be represented as follows

$$\left.\frac{\partial\left(NM_{\P}\right)}{\partial\P}\right|_{i,j} = \frac{\left(NM_{\P}\right)_{i+1/2,j} - \left(NM_{\P}\right)_{i-1/2,j}}{\Delta\P}$$
$$= \frac{N_{i+1/2,j}\left(\frac{M_{i+1,j} - M_{i,j}}{\Delta\P}\right) - N_{i-1/2,j}\left(\frac{M_{i,j} - M_{i-1,j}}{\Delta\P}\right)}{\Delta\P} \tag{23}$$
$$= \frac{N_{i+1/2,j}\left(M_{i+1,j} - M_{i,j}\right) - N_{i-1/2,j}\left(M_{i,j} - M_{i-1,j}\right)}{\left(\Delta\P\right)^2}$$

The term located at the cell interface found in Eq. (23) is computed through the method of averaging between two neighboring points. Thus, by adopting and expanding the procedure to other terms found in the viscous flux vectors as outlined beforehand, the second-order central difference approximation for the entire diffusion terms can be easily implemented.

As for time integration for the steady state problems, an explicit formulation is chosen for the current solver which utilizes a fourth-order Runge-Kutta method. Applying this method to the generalized two-dimensional RANS equations provides the following result

$$\bar{W}_{i,j}^{(1)} = \bar{W}_{i,j}^{n}$$
$$\bar{W}_{i,j}^{(2)} = \bar{W}_{i,j}^{n} - \frac{\Delta t}{4}\left[\left(\frac{\partial\bar{F}}{\partial\P}\right)_{i,j}^{(1)} + \left(\frac{\partial\bar{G}}{\partial\¦}\right)_{i,j}^{(1)} - \left(\frac{\partial\bar{F}_v}{\partial\P}\right)_{i,j}^{(1)} - \left(\frac{\partial\bar{G}_v}{\partial\¦}\right)_{i,j}^{(1)}\right]$$
$$\bar{W}_{i,j}^{(3)} = \bar{W}_{i,j}^{n} - \frac{\Delta t}{3}\left[\left(\frac{\partial\bar{F}}{\partial\P}\right)_{i,j}^{(2)} + \left(\frac{\partial\bar{G}}{\partial\¦}\right)_{i,j}^{(2)} - \left(\frac{\partial\bar{F}_v}{\partial\P}\right)_{i,j}^{(2)} - \left(\frac{\partial\bar{G}_v}{\partial\¦}\right)_{i,j}^{(2)}\right] \tag{24}$$
$$\bar{W}_{i,j}^{(4)} = \bar{W}_{i,j}^{n} - \frac{\Delta t}{2}\left[\left(\frac{\partial\bar{F}}{\partial\P}\right)_{i,j}^{(3)} + \left(\frac{\partial\bar{G}}{\partial\¦}\right)_{i,j}^{(3)} - \left(\frac{\partial\bar{F}_v}{\partial\P}\right)_{i,j}^{(3)} - \left(\frac{\partial\bar{G}_v}{\partial\¦}\right)_{i,j}^{(3)}\right]$$
$$\bar{W}_{i,j}^{n+1} = \bar{W}_{i,j}^{n} - \Delta t\left[\left(\frac{\partial\bar{F}}{\partial\P}\right)_{i,j}^{(4)} + \left(\frac{\partial\bar{G}}{\partial\¦}\right)_{i,j}^{(4)} - \left(\frac{\partial\bar{F}_v}{\partial\P}\right)_{i,j}^{(4)} - \left(\frac{\partial\bar{G}_v}{\partial\¦}\right)_{i,j}^{(4)}\right]$$

In order to save computing time; the viscous fluxes are only computed at the first stage of the Runge-Kutta scheme and frozen for the remaining stages [23, 24].

The finite difference approximation of the turbulence model in Eq. (10) and (11) is implemented in the following manners: the temporal term is discretized with a first-order forward difference scheme; the convective terms are approximated by a first-order upwind scheme; and a second-order central difference scheme, applied at cell interface is used for the remaining terms in the closure model. For algorithm modularity in the turbulence modeling, the set of k-ε / k-ω SST equations are lagged in time and solved separately from the RANS equations. To advance the solutions of the closure model, an Euler forward method is adopted together with the finite difference procedures as outlined previously.

4. Results and discussions

To validate the developed BGK turbulent flow solver, computations have been carried out for several benchmark test cases: supersonic turbulent flow over flat plate, supersonic transitional flow over flat plate, transonic turbulent flow over RAE2822 airfoil and Sajben transonic diffuser flow. Thus, numerical results for these test cases are presented in this section along with its relevant arguments against existing experimental or analytical data.

4.1. Supersonic turbulent flow over flat plate

The aim of this test case is to provide a platform to validate the solutions obtained from the developed BGK flow solver incorporated with a turbulence model (i.e. combined k-ε / k-ω SST) against experimental data provided by Erm et al. [25] and existing analytical solutions provided by Hoffmann and Chiang [21].

In this problem, an incoming fully turbulent supersonic flow is initiated in the free stream. The following free stream conditions are specified: Mach number M_∞ = 2.0, density ρ_∞ = 1.25 kg/m^3, temperature T_∞ = 300.0 K and Reynolds number Re_∞ = 3.762x10^6. The Reynolds number is based on a reference length taken as L_∞ = 0.08 m. A structure grid is created by an algebraic grid generation method with clustering near the surface and at the inlet to resolve high flow gradient areas. The resulting mesh has a size of 100 by 50 grid points and is shown in Fig. 1. As for the specification of conditions along the boundaries, the following are enforced: at left boundary the inflow conditions are specified as free-stream; at right and top boundaries, their conditions are determined by means of extrapolation from the interior domain; and the bottom boundary which locates the flat plate is set to assume adiabatic wall with no-slip conditions.

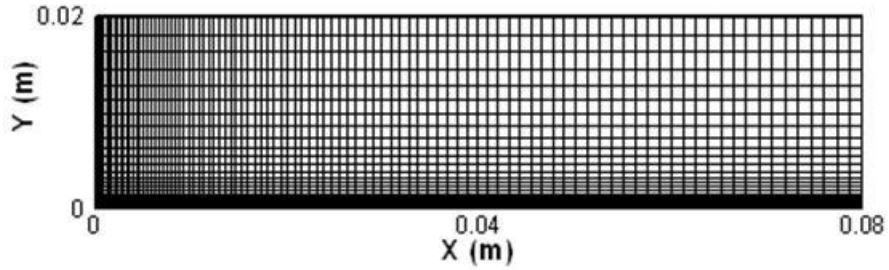

Figure 1. Computational domain for the flat plate

The flow quantities used as validation parameters consist of non-dimensional near wall velocity profile, boundary layer thickness distribution and surface skin friction coefficient along the plate. The computed velocity profile normal to the plate is shown in Fig. 2. The values depicted in the figure are taken at location corresponding to x = 0.06 m and normalized using the free stream conditions. As illustrated in the figure, the predicted velocity profile agrees very well with the experimental data taken from Ref. [25]. Figure 3 shows the shape of the boundary layer produced by the BGK flow solver. By comparing the computed boundary layer thickness with the analytical data, it can be deduced that the agreement between both results is excellent. For any viscous flow computation, it is always necessary to look at the resolution of the skin friction coefficient along the surface. Hence, the computed skin friction coefficient is compared with the analytical result taken from Ref. [21] and shown in Fig. 4. The computed result depicted in this figure shows that the BGK scheme slightly under-predicted the skin friction coefficient, especially in region between x = 0.01 m to x = 0.04 m but such prediction is considered satisfactory.

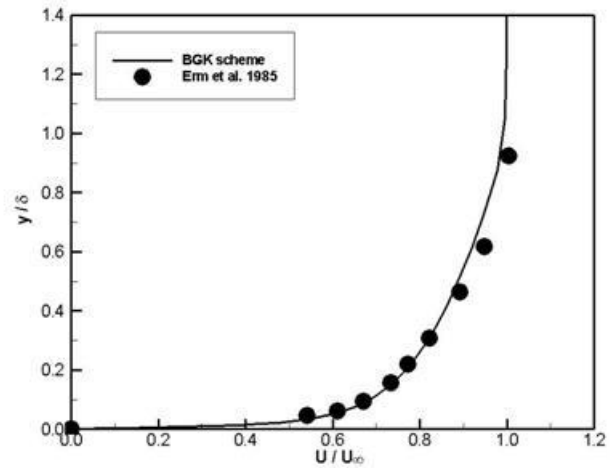

Figure 2. Near wall normalized velocity profile, taken at x = 0.06 m

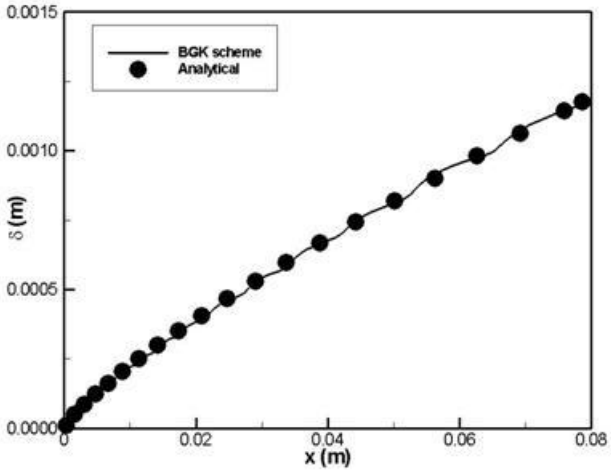

Figure 3. Boundary layer thickness distribution along the turbulent flat plate

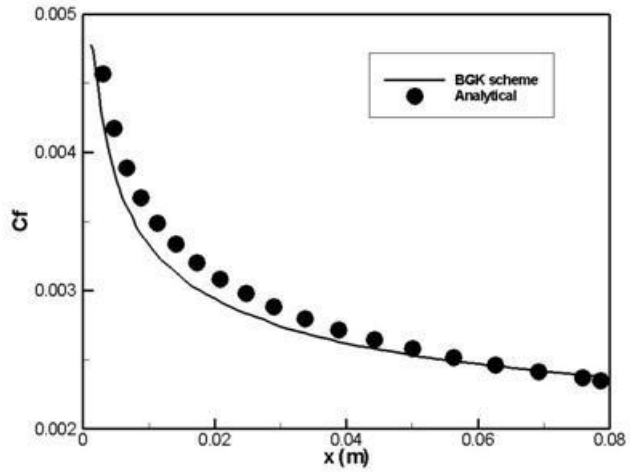

Figure 4. Skin friction coefficient along the surface of turbulent flat plate

4.2. Supersonic transitional flow over flat plate

This problem served to test the capability of the BGK flow solver to compute flow experiencing transitional in the flow domain. The computed results are validated with analytical data provided by Spalding and Chi [26].

An incoming supersonic laminar flow is initiated in the free stream. The transition to turbulent flow along the flat plate is artificially triggered and placed at 50 % of the plate length. The free stream conditions and mesh used for this test case are the same as given in the previous test case i.e. supersonic turbulent over flat plate. As for the specification of condition along the boundaries, the same set of conditions is applied.

The quantities computed via the numerical solvers that are presented for this test case consist of skin friction coefficient, non-dimensional velocity profile (located at x = 0.06 m), and boundary layer thickness, shown in Fig. 5-7. Through these figures, comparisons are made between the numerical results to the analytical data that will provide a good ground to assess the computational behavior of the solver. Figure 5 compares the skin friction coefficient distributions along the flat plate. The results depicted in this figure showed that the BGK scheme is capable of resolving the skin friction coefficient accurately prior to transition but with a slight over-prediction in the turbulent section of the flow where such a small percentage of disagreement in the prediction of transitional flow has been reported to be acceptable [21]. Next, the comparisons of non-dimensional velocity profiles located at x = 0.06 m is presented in Fig. 6. The illustrated results in this figure showed that a very good agreement can be seen between the numerical results and the analytical data. This deduction can also be applied and seen in Fig. 7 which illustrates the comparisons of boundary layer thicknesses.

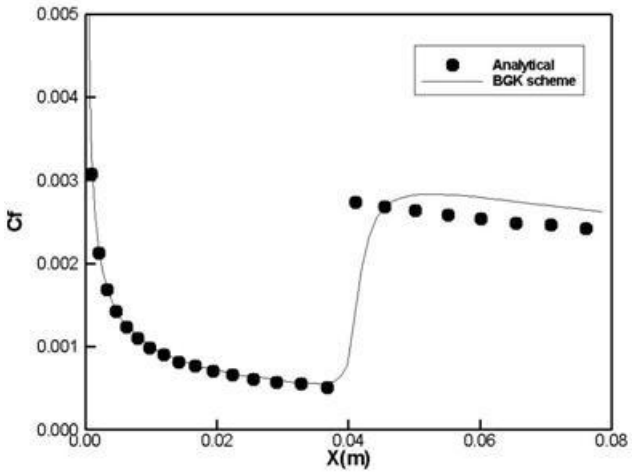

Figure 5. Skin friction coefficient for the transitional flat plate

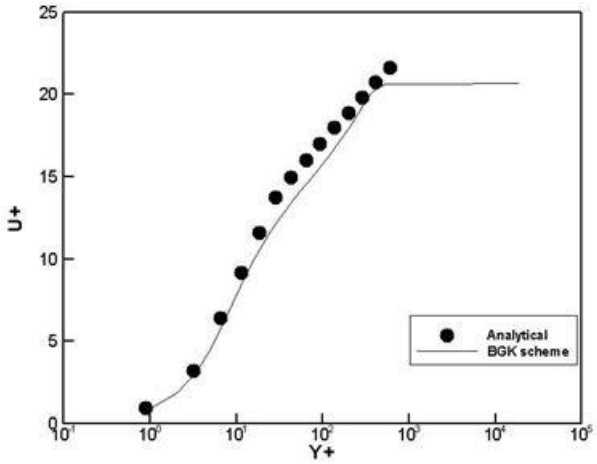

Figure 6. Velocity profiles for the transitional flat plate

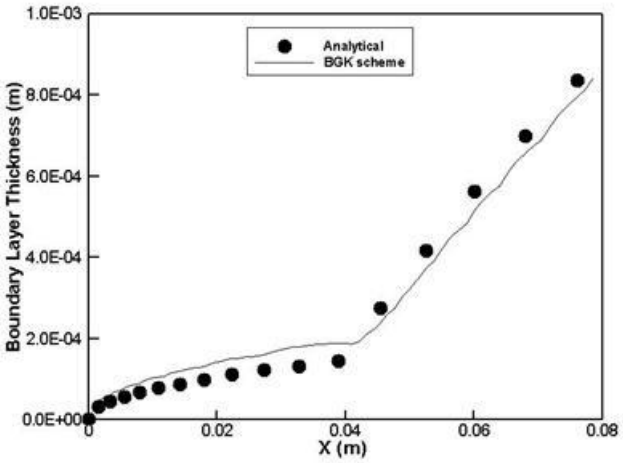

Figure 7. Boundary layer thickness for the transitional flat plate

4.3. Transonic turbulent flow over RAE2822 airfoil

The transonic flow over RAE2822 airfoil test case is selected in order to test the developed BGK flow solver incorporated with a turbulence model (i.e. combined k-ε / k-ω SST) to predict complex flow domain involving shock-boundary layer interaction. Extensive past tests and experimental data are available for this airfoil (i.e. [27-29]), thus making it an ideal test case to validate the computed results.

In this test case, flow conditions corresponding to AGARD test case 9 are used, namely, Mach number M_∞ = 0.73, Reynolds number Re_∞ = 6.5x10^6 and angle of attack α = 2.8^o. The free stream conditions used for initializing the flow domain are specified as: density ρ_∞ = 1.486 kg/m^3, temperature T_∞ = 255.6 K and reference length L_∞ = 0.3048 m. A structure C-grid with dimensions of 369 by 65 is generated by an algebraic grid generation method and is shown in Fig. 8 as zoom in view. As for the specification of conditions along the boundaries, the following are enforced: viscous wall boundary condition is applied at the airfoil surface; averaging boundary condition is used along the wake cut to provide continuous flow variables; free stream condition is applied at the outer boundary; the boundaries located on the right are applied with outflow condition where static pressure is fixed to the free stream pressure.

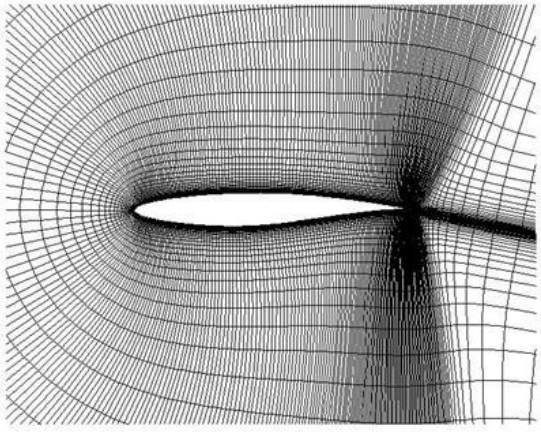

Figure 8. RAE2822 airfoil computational mesh, 369 x 65

The computed pressure contours are shown in Fig. 9, which predicts a shock-boundary layer interaction occurring at location about 60% of chord length on the upper surface of the airfoil. The computed pressure distribution is compared with the experimental data extracted from [27] in Fig. 10. The results illustrated in the figure show

that the rooftop pressure is accurately resolved and the pressure recovery which occurs after the shock is well predicted with remarkable accuracy. However, the shock location is slightly predicted downstream in comparison to the experimental data. The computed skin friction coefficient distribution along the airfoil surface is compared with experimental data from [27] and shown in Fig. 11. The resolution of the skin friction coefficient on the upstream side of the shock location on the top side of the airfoil surface is predicted with great accuracy. In addition, the skin friction coefficient is slightly over-predicted in the region after the shock. No detailed comment can be made with regards to the skin friction coefficient on the bottom side of the airfoil surface because there is just one experimental data point available in that region.

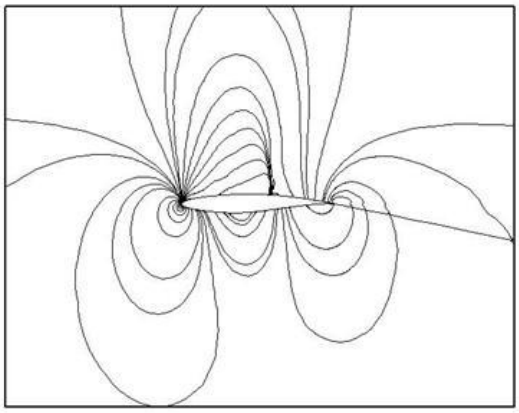

Figure 9. Pressure contours near the RAE2822 transonic airfoil

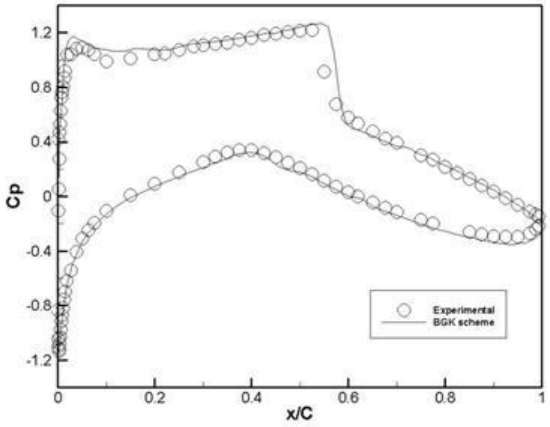

Figure 10. Pressure coefficient distribution on the RAE2822 airfoil

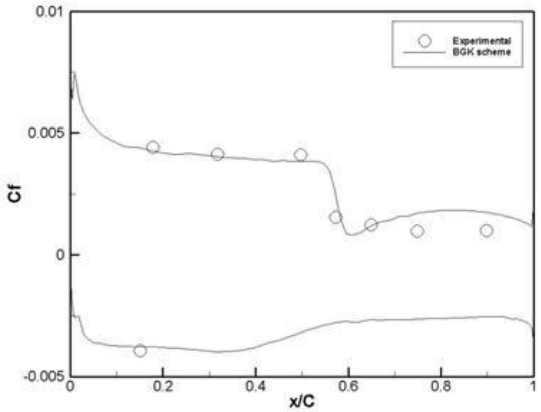

Figure 11. Skin friction coefficient distribution on the RAE2822 airfoil

4.4. Sajben transonic diffuser flow

The computation of transonic turbulent diffuser flows have been implemented in this study using the developed BGK turbulent flow solver. This two-dimensional convergent-divergent channel acts to simulate the types of flows that may exist in supersonic inlets of aircraft engines. Extensive tests, both numerical and experimental have been conducted at a variety of flow conditions for this geometry. Hence, validation data (i.e. Ref. [18, 19, 30-32]) are plentiful and can be readily used to the advantage of current study to further test the computational characteristic of the solver when dealing with this sort of complex flow. The flow fields selected for the current study are the weak- and strong-shock diffuser cases of Sajben [32].

For this test case, fully turbulent subsonic flow is initiated in the free stream with the following free stream conditions: Mach number $M_\infty = 0.46$, density $\rho_\infty = 1.45$ kg/m^3, temperature $T_\infty = 280.1$ K and Reynolds number $Re_\infty = 0.5634 \times 10^6$. The Reynolds number is based on the converging-diverging duct throat's height which is measured as $L_\infty = 0.044$ m. A structure algebraic grid is generated with clustering enforced on both surfaces of the channel. The resulting mesh has a size of 81 by 51 grid points and is shown in Fig. 12. As for the specification of boundary conditions, the following are assumed: at left boundary, subsonic inflow condition with extrapolated static pressure from the interior domain; at right boundary, subsonic outflow condition with fixed static pressure; the top and bottom boundaries which locate the surface, are set to assume adiabatic wall with no-slip condition. The fixed static pressure required at the outflow boundary depends on the type of flow field needed to be modeled, i.e. weak-shock or strong shock flow. The specified pressure ratio ($P_{ratio} = P_{exit} / P_{total,\ inlet}$) is 0.82 and 0.72 for weak-shock and strong-shock flows, respectively.

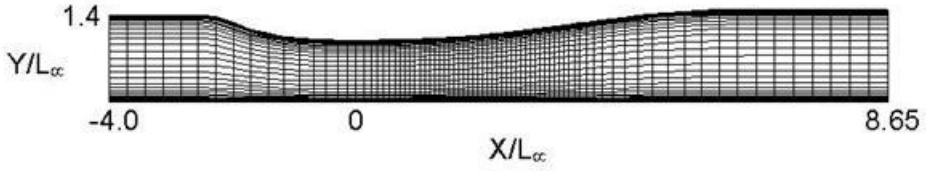

Figure 12. Sajben diffuser computational domain, 81 x 51

For both flow conditions, pressure distributions along the top and bottom walls of the diffuser from the BGK solver computations are compared with the experimental pressures and shown in Fig. 13-16. In general, all computed pressure distributions agree relatively well with the experimental data. Figure 13 and 14 illustrate the pressure distribution produced from the weak-shock simulation. As illustrated in the figures, the predicted pressure distributions agree very well with the experimental data with the location of the shock resolve accurately. Next, the computed results of the strong-shock case are considered. Similar to the weak-shock case, the pressure distributions on both surfaces of the channel are compared against the experimental pressure, i.e. Fig. 15 and 16. Again, the predicted results are comparable with the experimental data. The shock location for the bottom wall is predicted with great accuracy, but the top wall shock is slightly under-predicted and 1 grid point further downstream as seen in Fig. 16. Nonetheless, this level of inaccuracy in the solutions can be considered satisfactory considering the coarseness of the mesh used in the computation and also large separation that occurred on the top wall.

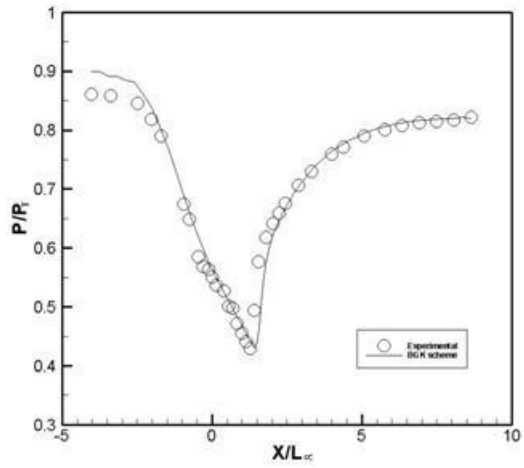

Figure 13. Bottom wall pressure distribution, weak-shock case (P_{ratio} = 0.82)

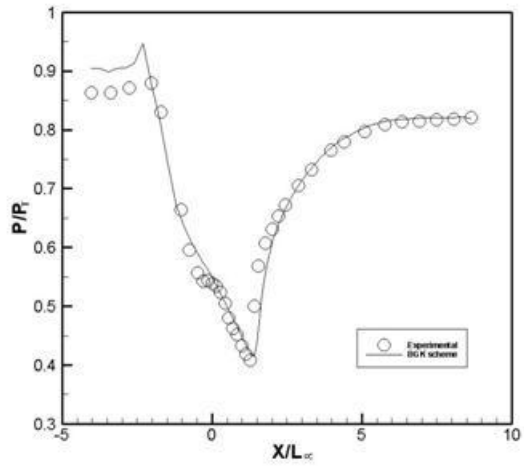

Figure 14. Top wall pressure distribution, weak-shock case (P_{ratio} = 0.82)

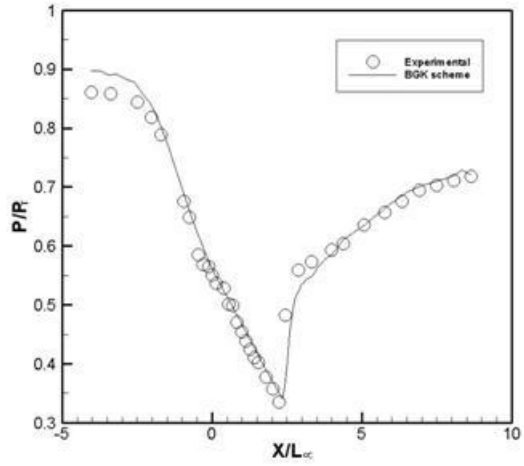

Figure 15. Bottom wall pressure distribution, strong-shock case (P_{ratio} = 0.72)

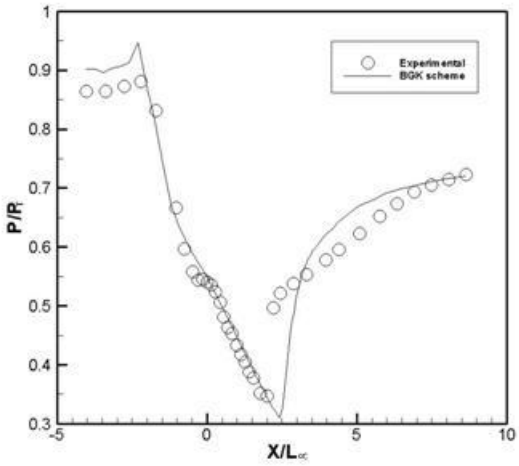

Figure 16. Top wall pressure distribution, strong-shock case (P_{ratio} = 0.72)

5. Conclusion

In the present work, the *k-ε* / *k-ω* SST two-equation turbulence model has been successfully incorporated into the existing BGK flow solver developed in the previous study. Validation test cases conducted in this paper showed that the BGK turbulent flow solver is capable of simulating turbulent flow that gives good results for a wide variety of flows, i.e. ranging from simple to complex flow domain; from subsonic to supersonic flow; and flow fields involving shock-boundary layer interaction. In some test cases (i.e. RAE2822 airfoil and Sajben diffuser), the computed results clearly demonstrate that the BGK scheme is able to provide an accurate resolution of the flow, good prediction of shock location and remarkable post shock recovery of flow variables. These claims are justified by comparisons of the numerical findings of the BGK scheme with existing analytical and experimental data via examining the relevant flow properties.

Nomenclature

C_f	skin friction coefficient
F, G	inviscid flux vector in Cartesian coordinates
F_v, G_v	viscous flux vector in Cartesian coordinates
$\bar{F}, \bar{G}$	inviscid flux vector in generalized coordinates
$\bar{F}_v, \bar{G}_v$	viscous flux vector in generalized coordinates
i, j	grid point location in computational domain
k	turbulent kinetic energy
M_∞	free stream Mach number
n	time level
P_T	inlet total pressure
Re_∞	free stream Reynolds number
U_c, V_c	contravariant velocity
W	conservative variables in Cartesian coordinates
$\bar{W}$	conservative variables in generalized coordinates
γ	specific heat ratio
δ	boundary layer thickness
ε	dissipation rate of turbulent kinetic energy
ω	specific dissipation rate
Δt	time step
$\Delta\xi$, $\Delta\eta$	spatial step in generalized coordinates

Acknowledgements

The authors would like to acknowledge the support of the International Islamic University Malaysia (IIUM) through Research Management Center under the grant No. EDW B-0702-32 and Universiti Teknologi MARA (UiTM) through Research Management Institute under the grant No. 600-RMI/ST/FRGS 5/3/Fst(179/2010).

References

[1] K. Xu, "Gas-Kinetic Scheme for Unsteady Compressible Flow Simulations," Von Kármán Ins. for Fluid Dynamics Lecture Series, vol. 1998-03, Von Kármán Ins., Rhode St. Genese, Belgium, 1998.

[2] J. C. Ong, "Computational Analysis of Gas-Kinetic BGK Scheme for Inviscid Compressible Flow," M. Sc. Thesis, University Putra Malaysia, Malaysia, 2004.

[3] J. C. Ong, A. A. Omar, W. Asrar, and M. M. Hamdan; "Development of Gas-Kinetic BGK Scheme for Two-Dimensional Compressible Inviscid Flows," AIAA Paper 2004-2708, 2004.

[4] K. Xu, "Gas-Kinetic Theory Based Flux Splitting Method for Ideal Magnetohydrodynamics," ICASE Report, 98-53, Nov. 1998.

[5] D. S. Chae, C. A. Kim, and O. H. Rho, "Development of an Improved Gas-Kinetic BGK Scheme for Inviscid and Viscous Flows," Journal of Computational Physics, Vol. 158, pp. 1-27, 2000.

[6] J. C. Ong, A. A. Omar, and W. Asrar, "Evaluation of Gas-Kinetic Schemes for 1D Inviscid Compressible Flow Problem," International Journal of Computational Engineering Science (IJCES), Vol. 4, No. 1, pp. 829-851, Dec. 2003.

[7] J. C. Ong, A. A. Omar, W. Asrar, and M. M. Hamdan, "An Implicit Gas-Kinetic BGK Scheme for Two-Dimensional Compressible Inviscid Flows," AIAA Journal, Vol. 42, No. 7, pp 1293-1301, 2004.

[8] J. C. Ong, A. A. Omar, W. Asrar, and Z. A. Zaludin, "Gas-Kinetic BGK Scheme for Hypersonic Flow Simulation," AIAA Paper, 2006-0990, Jan. 2006.

[9] S. N. Addusslam, J. C. Ong, M. M. Hamdan, A. A. Omar, and W. Asrar, "Application of Gas-Kinetic BGK Scheme for Solving 2-D Compressible Inviscid Flow around Linear Turbine Cascade," Int. Journal for Computational Methods in Engineering Science and Mechanics, Vol. 7, No. 6, Nov. 2006.

[10] G. May, B. Srinivasan and A. Jameson, "An Improved Gas-Kinetic BGK Finite-Volume Method for Three-Dimensional Transonic Flow," Journal of Computational Physics, Vol. 220, Issue 2, pp. 856-878, 2007.

[11] S. Q. Zhang, M. S. Ghidaoui, W. G. Gray and N. Z. Li, "A Kinetic Flux Vector Splitting Scheme for Shallow Water Flows," Advances in Water Resources, Vol. 26, pp. 635-647, 2003.

[12] K. Xu, M. Mao and L. Tang, "A Multidimensional Gas-Kinetic BGK Scheme for Hypersonic Viscous Flow," Journal of Computational Physics, Vol. 203, Issue 2, pp. 405-421, 2005.

[13] K. S. Ravichandran, "Higher Order KFVS Algorithms using Compact Upwind Difference Operators," Journal of Computational Physics, Vol. 130, Issue 2, pp. 322-334, 1997.

[14] A. A. Omar, J. C. Ong, W. Asrar and A. F. Ismail, "Accuray of Bhatnagaar-Gross-Krook Scheme in Solving Laminar Viscous Flow Problems," AIAA Journal, Vol. 47, No. 4, pp 885-892, 2009.

[15] A. Leonard, "Energy Cascade in Large-Eddy Simulations of Turbulent Fluid Flows," Advances in Geophysics, Vol. 18A, pp. 237-248, 1974.

[16] Z. Liu, W. Zhao and C. Liu, "Direct Numerical Simulation of Transition in a Subsonic Airfoil Boundary Layer," AIAA-97-0752, January, 1997.

[17] F. F. Hatay and S. Biringen, "Direct Numerical Simulation of Low-Reynolds Number Supersonic Turbulent Boundary Layers," AIAA-95-0581, January, 1995.

[18] K. C. Ng, M. Z. Yusoff and T. F. Yusaf, "Simulations of Two-Dimensional High Speed Turbulent Compressible Flow in a Diffuser and a Nozzle Blade Cascade," American Journal of Applied Sciences 2 (9), pp. 1325-1330, 2005.

[19] N. J. Georgiadis, J. E. Drummond and B. P. Leonard, "Evaluation of Turbulence Models in the PARC Code for Transonic Diffuser Flows," AIAA-94-0582, January, 1994.

[20] K. A. Hoffmann and S. T. Chiang, "Computational Fluid Dynamics for Engineers," Engineering Education System, Wichita, Vol. 2, Chap. 11 and 14, 1993.

[21] K. A. Hoffmann and S. T. Chiang, "Computational Fluid Dynamics for Engineers," Engineering Education System, Wichita, Vol. 3, Chap. 21, 2000.

[22] C. Hirsch, "The Numerical Computation of Internal and External Flows," John Wiley & Sons, New York, Vol. 2, Chap. 21, 1990.

[23] A. Jameson, W. Schmidt and E. Turkel, "Numerical Solutions of the Euler Equations by Finite Volume Methods using Runge-Kutta Time Stepping Schemes," AIAA 81-1259, 1981.

[24] P. Niyogi, S. K. Chakrabartty and M. K. Laha, "Introduction to Computational Fluid Dynamics," Pearson Education, Singapore, Chap. 13, 2005.

[25] L. P. Erm, A. J. Smits and P. N. Joubert, "Low Reynolds number turbulent boundary layers on a smooth flat surface in a zero pressure gradient," Proc. 5th Symp. on Turbulent Shear Flows, Ithaca, NY, August 7-9, 1985.

[26] D. B. Spalding and S. W. Chi, "The drag of a compressible turbulent boundary layer on a smooth plate with and without heat transfer," J. of Fluid Mechanics, Vol. 18, No. 1, pp 117-143, 1964.

[27] F. S. Lien, G. Kalitzin, and P. A. Durbin, "RANS modeling for compressible and transitional flows," Center for Turbulence Research summer proceedings, pp. 267-286, 1998.

[28] J. W. Slater, "RAE2822 Transonic Airfoil: Study #1," NASA Glenn Research Centre, Ohio. Internet: http://www.grc.nasa.gov/WWW/wind/valid/raetaf/raetaf01/raetaf01.html

[29] J. P. Singh, "An improved Navier-Stokes flow computation of AGARD Case-10 flow over RAE2822 airfoil using Baldwin-Lomax model," Acta Mechanica, Vol. 151, pp. 255-263, 2001.

[30] Q. Xiao and H. M. Tsai, "Computation of Transonic Diffuser Flows by a Lagged k-ω Turbulence Model," Journal of Propulsion and Power, Vol. 19, No. 3, 2003.

[31] T. T. Bui, "Implementation/Validation of a Low Reynolds Number Two-Equation Turbulence Model in the Proteus Navier-Stokes Code – Two-Dimensional/Axisymmetric," NASA Technical Memorandum 105619, 1992.

[32] D. Yoder, "Sajben Transonic Diffuser: Study #2," NASA Glenn Research Centre, Ohio. Internet: http://www.grc.nasa.gov/WWW/wind/valid/transdif/transdif02/transdif02.html